National Centre for Radio Astrophysics

Internal Technical Report
GMRT/R309
15Jun2022

uGMRT 2D primary beam measurements @ L band

Santaji N. Katore and Jayaram N. Chengalur

NCRA - GMRT - TIFR

uGMRT 2D primary beam measurements @ L-Band

Santaji N. Katore and Jayaram N. Chengalur
NCRA-GMRT-TIFR

Abstract

In interferometric images, knowledge of the primary beam is important for the measurement of fluxes and spectra of sources away from the pointing centre. Correction for the effect of the varying primary beam sensitivity is also important in high dynamic imaging. Here, we present first measurements the frequency dependent primary beam shapes for band-5 (L-band, 1060 – 1460 MHz) of the upgraded GMRT. These measurements would form a useful input for all uGMRT users.

Introduction/Motivation

The recently completed GMRT upgrade (Gupta et al. 2019) has resulted in a significant increase in the instantaneous bandwidth of the telescope. This, it turn, leads to a significant increase in the sensitivity for continuum as well as pulsar studies. As part of the upgrade, all the antenna feeds, except the L-band feed have been replaced. The L-band feed is the same as for the pre-upgrade GMRT. Earlier measurements of the primary beam shape at L-band however were available only in the form of the best fit polynomial to an assumed azimuthally symmetric beam. Here we provide measurements of the actual 2-D shape of the beam in each polarization. The beam is significantly azimuthally asymmetric, as well as different for the two polarizations. The stokes I beam (i.e. the sum of the beams of the two polarizations) is however reasonably azimuthally symmetric, and for applications in which it is sufficient to assume an azimuthally symmetric polarization independent beam, we also provide polynomial fits to the same.

Experimental procedure for data collection

The observations for determining the beam shape were made in the interferometric mode, using observations of 3C sources (3C286, 3C48 and 3C147). The default frequency setup for continuum L-band observations was used for all observations. (Bandwidth = 400 MHz, Num. of Channels = 1024, Frequency Range = 1060 – 1460 MHz., GAB LO = 1460 MHz.). The antennas were scanned in the azimuth axis, with the multiple scans spaced 3’ apart along the elevation axis. The scan rate was 30’/minute and the integration time was either 2 or 4 seconds. The total grid size was selected to cover the beam at least up to the first null. For high dynamic range imaging applications one would need to determine the primary beam to still further distances than what our measurements provide. One would also need to know the full polar properties of the beam. As such, our measurements should be regarded only as a first step in the direction of characterising the primary beam. We also note that the current feed positioning system at the GMRT has limited accuracy. This results in different primary beam shapes every time a feed is brought to focus. As such, it may, in any case be difficult to apply the high dynamic range imaging techniques that use information about the primary beam. The current measurements may hence be adequate, at least at the L-band, until the feed position system is upgraded. (The upgrade which is expected to provide much better repeatability in feed positioning is currently under way, and is expected to finish shortly).

Note on the nomenclature

The Band 5 feeds at the GMRT are linearly polarized, and should correctly be labeled "XX" and "YY". However, for historical reasons (mainly compatibility with the nomenclature at other frequencies) they have been called "RR" and "LL" at the GMRT. We continue with this labeling here. For similar reasons, stokes I is labeled "RRLL" in all plots.

Data analysis

After flagging out non functional antennas, the visibilities were used to determine antenna based gains, which were squared to get the power. The antenna gain solution was computed independently for ~ 0.39 MHz wide channels spaced ~ 5 MHz apart to cover the frequency range from 1060 MHz to 1460 MHz. The known raster scan rate and elevation position were used to convert the timestamp of the data into the position on in the grid. Gnuplot was used to interpolate the observations onto a uniform grid in altitude and azimuth for each polarization. 2D elliptical Gaussians were fit to each data set using gnuplot to parameterize the beam shape. This parameterization is used to study the variation of the beam with frequency and polarization. Specifically the 2D beam data grid was parametrized using a function of the form:

$$f(x,y)=A\exp(-(a(x-x_o)^2+2b(x-x_o)(y-y_o)+c(y-y_o)^2)) \quad \text{...(1)}$$

where,

$$a=\frac{\cos^2\theta}{2\sigma_M^2}+\frac{\sin^2\theta}{2\sigma_m^2}$$

$$b=\frac{-\sin 2\theta}{4\sigma_M^2}+\frac{\sin 2\theta}{4\sigma_m^2}$$

$$c=\frac{\sin^2\theta}{2\sigma_M^2}+\frac{\cos^2\theta}{2\sigma_m^2}$$

Here the coefficient A is the amplitude, x_o, y_o are the offsets from the center and σ_M *and* σ_m are the major and minor axis of the beam, (see below). The angle θ indicates the position angle in case of an elliptical beam.

$$\mathrm{HPBW} = \sigma_M \;\; (2.35482) \quad \ldots.. \quad \textit{for major axis}$$
$$\mathrm{HPBW} = \sigma_m \;\; (2.35482) \quad \ldots... \quad \textit{for minor axis}$$

Each Gaussian is normalized to unity at the peak and the peak position was also set to (0,0), i.e. the origin. This is to correct for any pointing offsets in the individual antennas. As such, the measurement here is meant to indicate the “typical” antenna beam.

As an example, Fig (1) shows the Gaussian fits for W02 antenna at 1080 MHz for the RR abd LL polarizations. As can be seen the beams are somewhat elliptical, and the major axis of the RR and LL beams are approximately at right angles to one another. As discussed further below, this is typical for the GMRT band 5 feed.

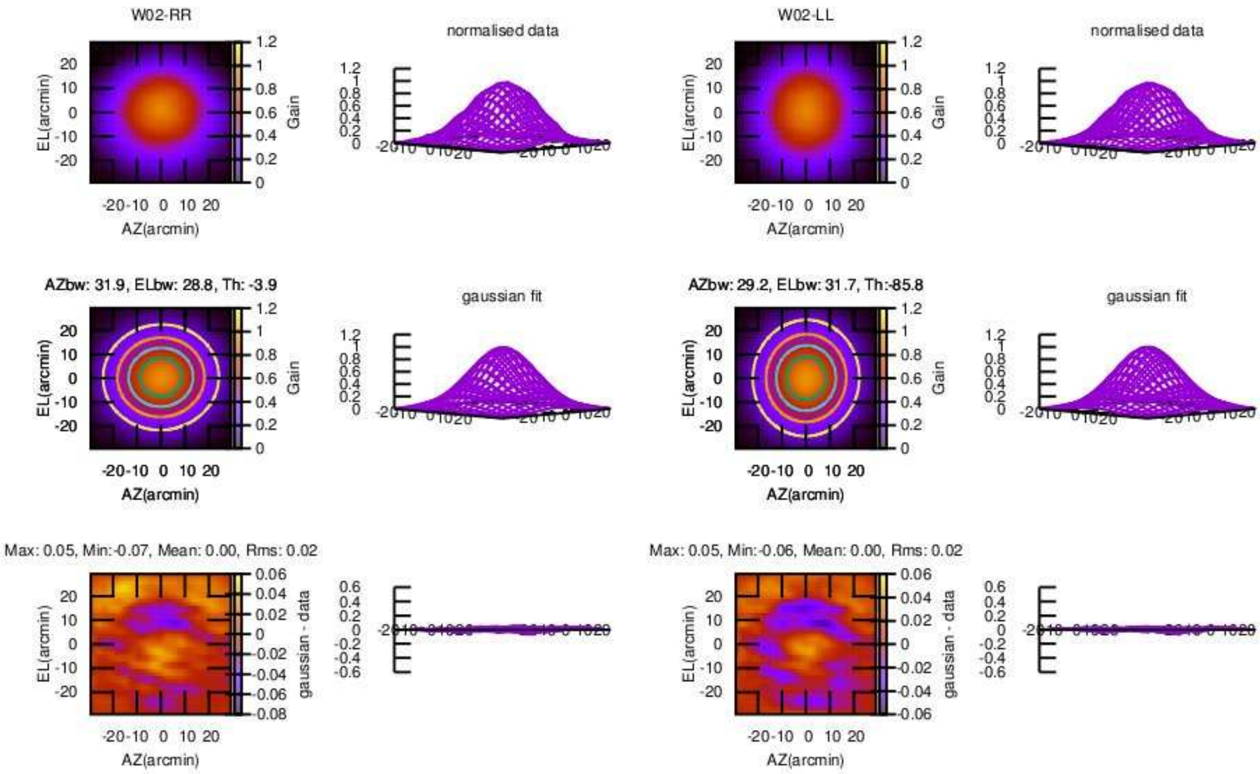

Fig(1)

All the gridded data for the good antennas were averaged together (pixel by pixel) to form a single average data set for a given observation. This was done separately for the RR and LL polarizations at each frequency setting. In addition a stokes I beam was generated by averaging the RR and LL data for each polarization.

A total of 6 such observations were made spread over the period from 25 Dec 2017 to 10 Feb 2019. In addition to the per observation average computed as described above, an average over all observations (labeled “AVG”) as well as a median over all observations (labeled “MED”) were also computed over all the 6 data sets.

Systematic trends in the measurements

Beam Ellipticity

Fig (2) shows the plot of the HPBW measured from the MED beam as a function of frequency. The three different colored points indicates the RR (i.e. X polarization, red), LL (, i.e. Y polarization, green) and RRLL (, i.e. stoke I, blue). The solid circles are for the AZ axis while the empty ones are for the EL axis. Missing points in the plots are due to the removal of RFI affected data.

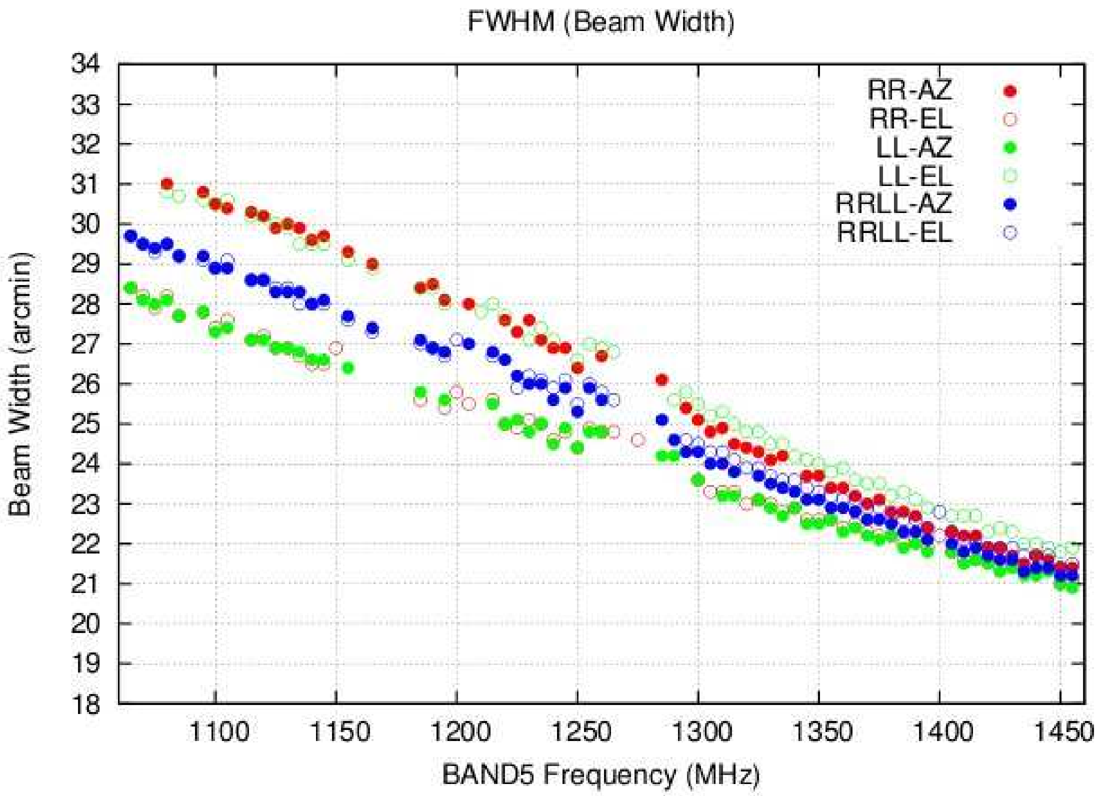

Fig(2)

As can be seen the RR and LL beams are elliptical, with the ellipticity being more pronounced at the lower frequencies. The fractional difference between the FWHM along the major and minor axis varies from about 5% at 1450 MHz to about 10% at 1000 MHz. The major axis of the two ellipses are also mis-aligned, with one beam being wider along the elevation axis and the other being wider along the azimuth axis. On the other hand the stokes I ("RRLL") beam has close to equal widths along the elevation and azimuth axis.

Scaling with Frequency

Naively one would expect the beam width to scale linearly with wavelength. However, since the feed illumination may vary in a non trivial manner with wavelength, deviations from this simple scaling are possible. We hence did fits of both first and second order polynomials to the major axis HPBW as a function of frequency, viz.

First Order Polynomial: $f(x) = \lambda / a_1$
Second Order Polynomial: $f(x) = \lambda / a_1 + \lambda^2 / a_2$

Where λ is wavelength and a_1 and a_2 are the polynomial coefficients.

Fig(3) shows the first order polynomial fit to the beam width(RRLL) and Fig(4) shows the second order fit to the beam width (RRLL). The fits (Fig 3) indicate that the second order fit is somewhat better that the first order fit

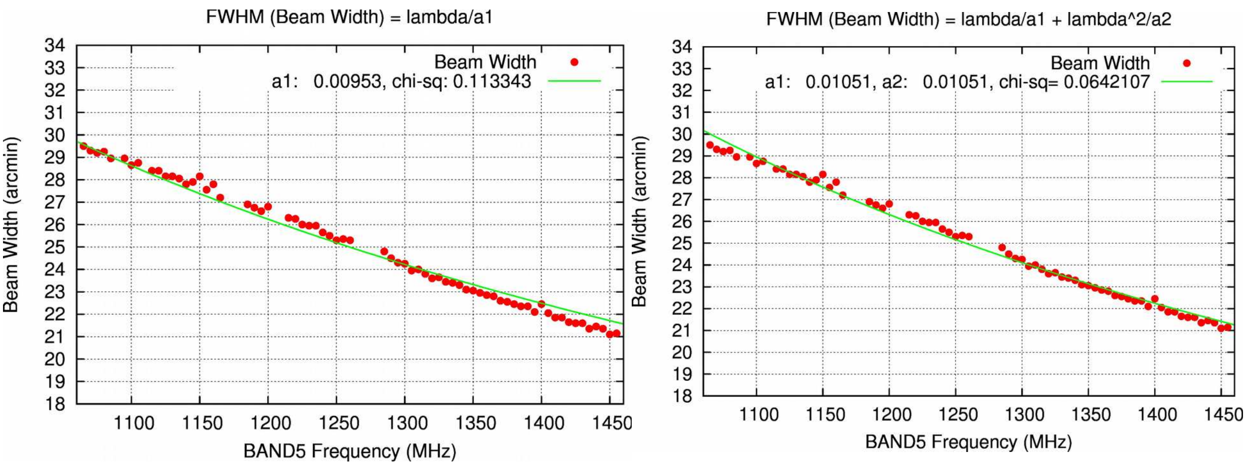

Fig(3)

Azimuthally symmetric fits

As discussed above, the stokes I beam can be reasonably well approximated to be azimuthally symmetric. For applications in which this approximation is sufficent we provide below 8th, 10th and 12th order polynomial fits to the beam.

The 8th order polynomial function is expressed as

$$f(x,y)=1+(\frac{a}{10^3})(r\nu)^2+(\frac{b}{10^7})(r\nu)^4+(\frac{c}{10^{10}})(r\nu)^6+(\frac{d}{10^{13}})(r\nu)^8 \qquad \ldots(2)$$

The 10th order polynomial function is expressed as

$$f(x,y)=1+(\frac{a}{10^3})(r\nu)^2+(\frac{b}{10^7})(r\nu)^4+(\frac{c}{10^{10}})(r\nu)^6+(\frac{d}{10^{13}})(r\nu)^8+(\frac{e}{10^{16}})(r\nu)^{10} \quad \ldots(3)$$

The 12th order polynomial function is expressed as

$$f(x,y)=1+(\frac{a}{10^3})(r\nu)^2+(\frac{b}{10^7})(r\nu)^4+(\frac{c}{10^{10}})(r\nu)^6+(\frac{d}{10^{13}})(r\nu)^8+(\frac{e}{10^{16}})(r\nu)^{10}+(\frac{f}{10^{19}})(r\nu)^{12} \quad .(4)$$

where,

$$r=\sqrt{(x^2+y^2)}$$

here r is the separation from pointing position in arc-min, ν is the frequency in GHz, *a, b, c, d, e and f* are the polynomial coefficients. Fig. (5) and (6) show the average and the median RRLL beams, as well as the corresponding model beams and the difference between the data and the model.

Figs. (7), (8) and (9) show the polynomial coefficients as a function of frequency for the order 8th, 10th and 12th respectively. The coefficients themselves are also listed at the end of this report.

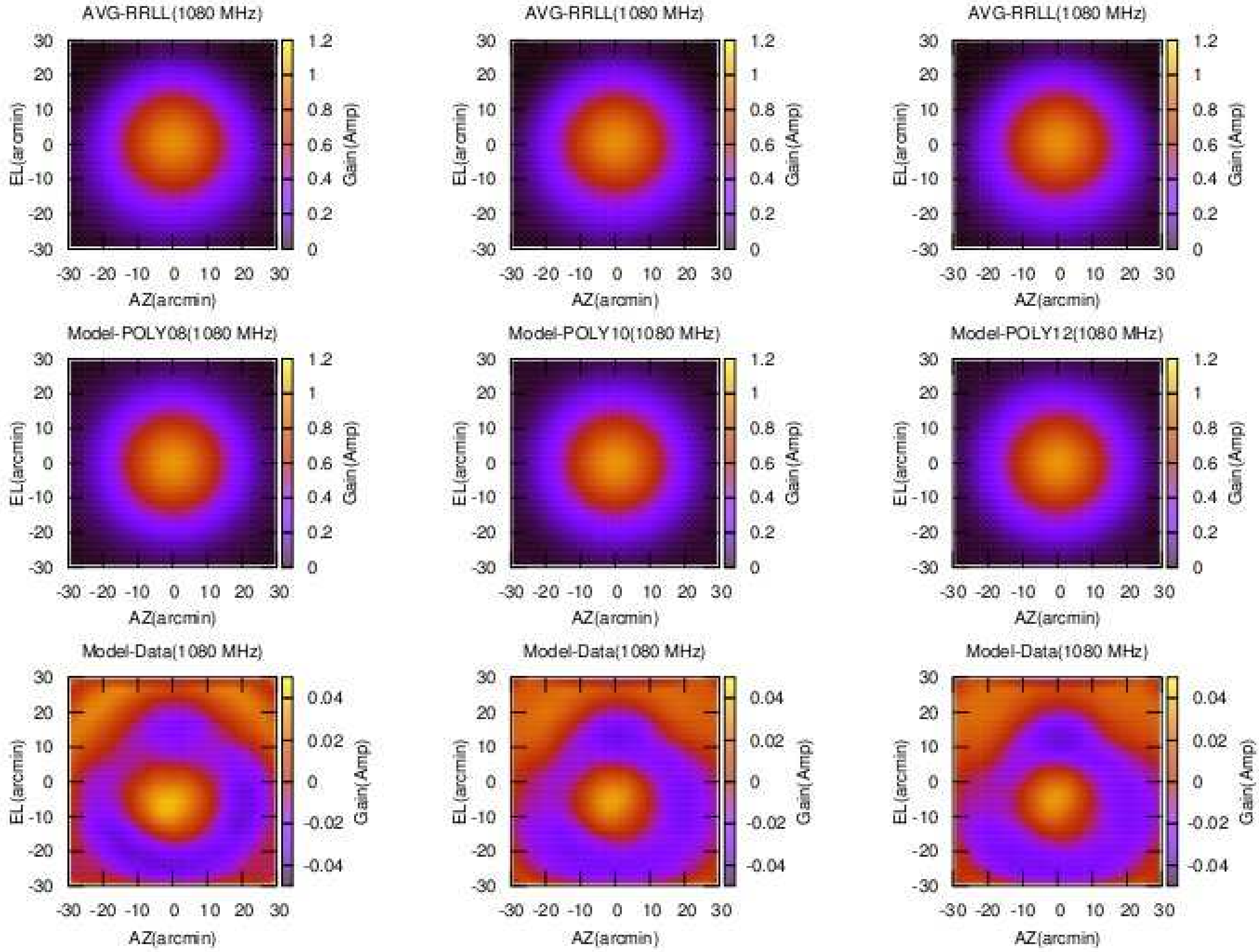
AVG-RRLL(1080 MHz)
AVG-RRLL(1080 MHz)
AVG-RRLL(1080 MHz)
Model-POLY08(1080 MHz)
Model-POLY10(1080 MHz)
Model-POLY12(1080 MHz)
Model-Data(1080 MHz)
Model-Data(1080 MHz)
Model-Data(1080 MHz)
EL(arcmin)
AZ(arcmin)
Gain(Amp)

Fig(5)

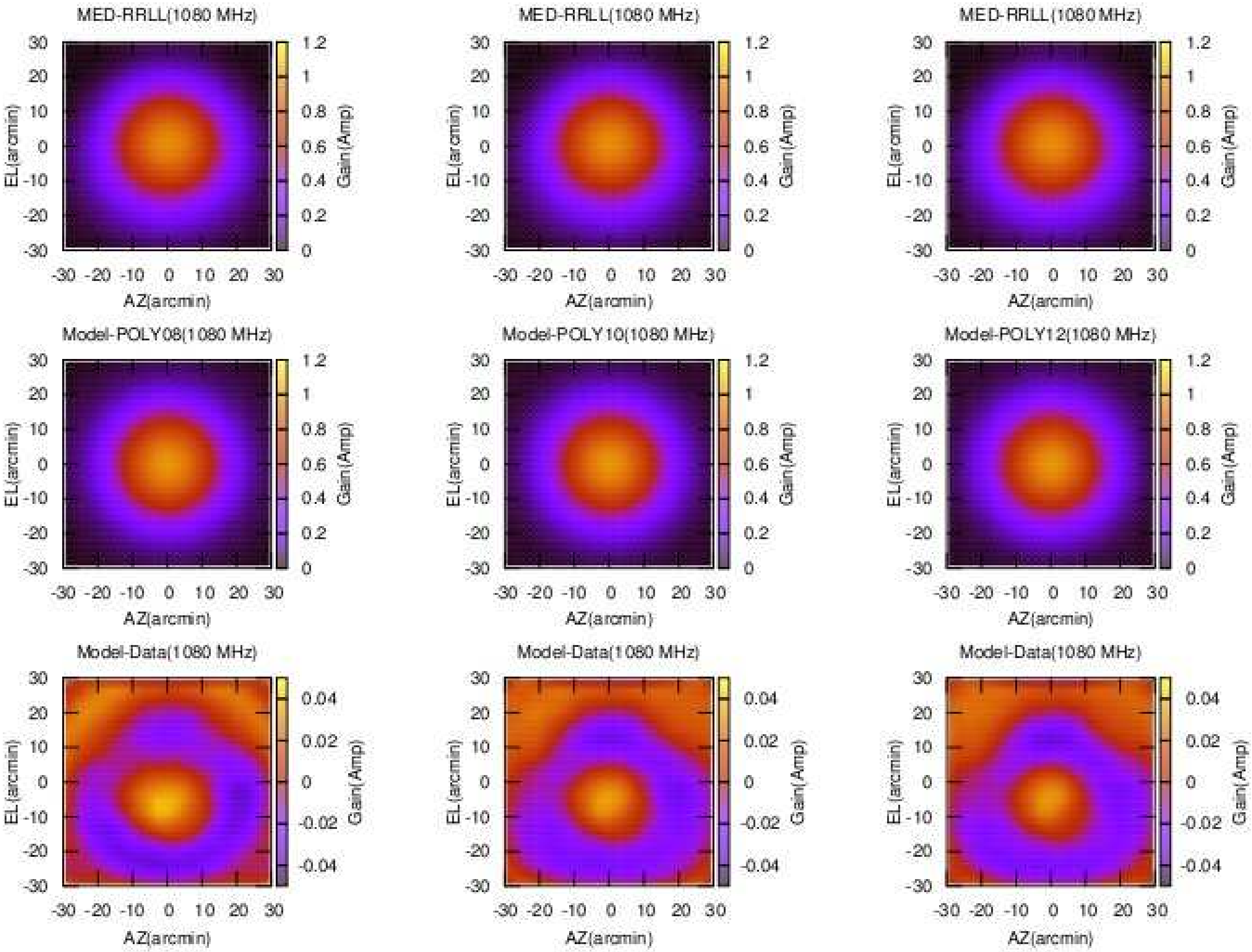
MED-RRLL(1080 MHz)
MED-RRLL(1080 MHz)
MED-RRLL(1080 MHz)
Model-POLY08(1080 MHz)
Model-POLY10(1080 MHz)
Model-POLY12(1080 MHz)
Model-Data(1080 MHz)
Model-Data(1080 MHz)
Model-Data(1080 MHz)
EL(arcmin)
AZ(arcmin)
Gain(Amp)

Fig(6)

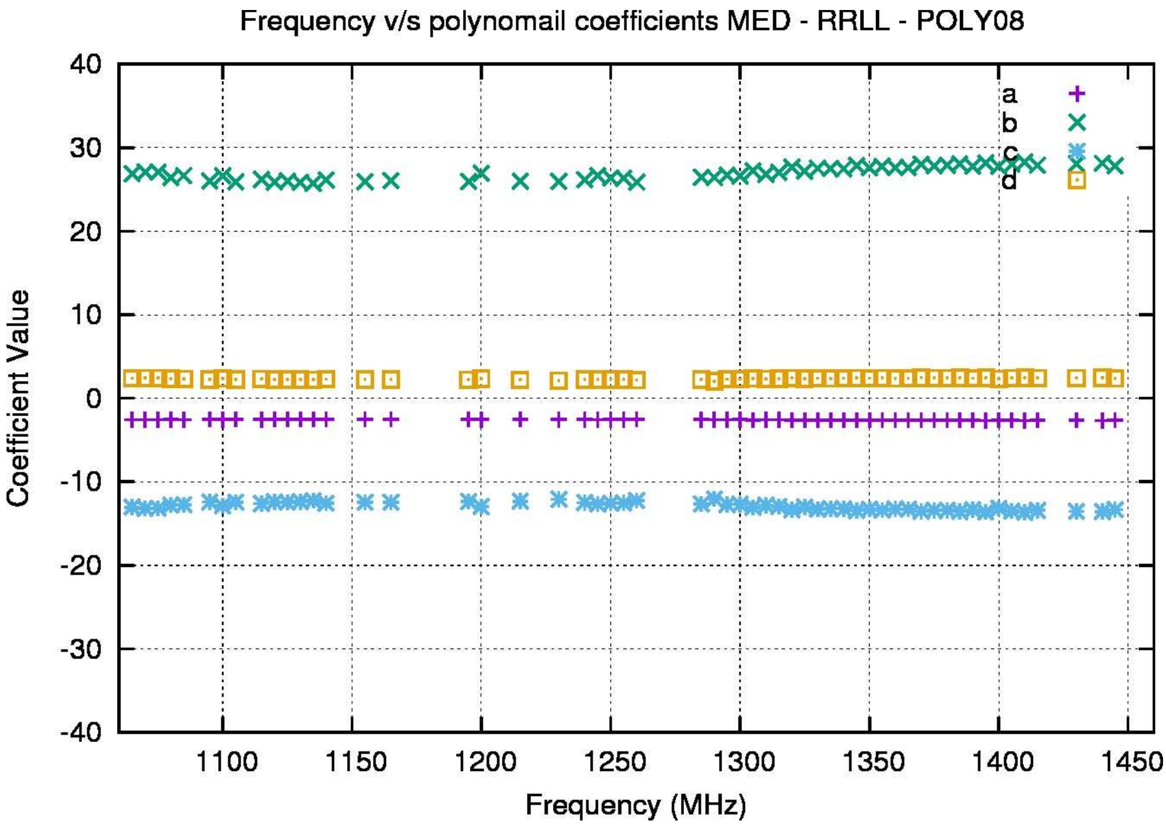
Frequency v/s polynomail coefficients MED - RRLL - POLY08
Coefficient Value
Frequency (MHz)
a
b
c
d
40
30
20
10
0
-10
-20
-30
-40
1100
1150
1200
1250
1300
1350
1400
1450

Fig(7)

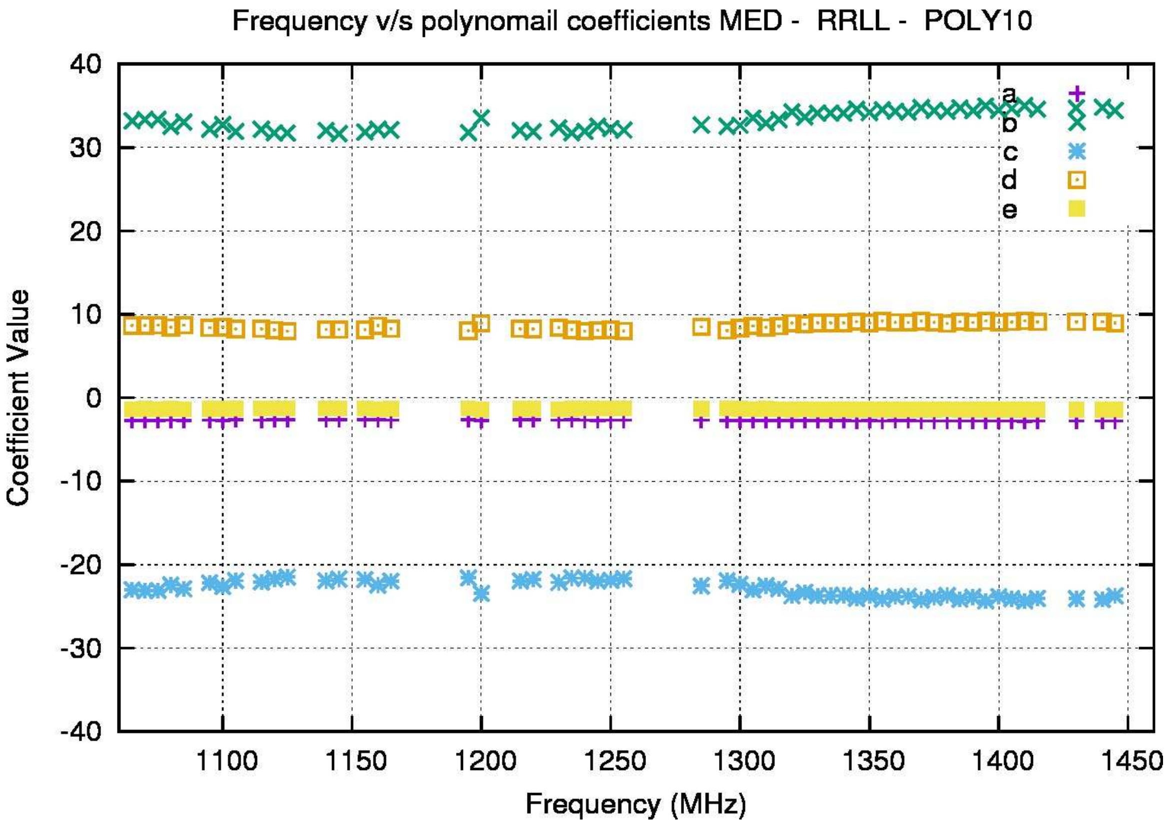
Frequency v/s polynomail coefficients MED - RRLL - POLY10
Coefficient Value
Frequency (MHz)
a
b
c
d
e
40
30
20
10
0
-10
-20
-30
-40
1100
1150
1200
1250
1300
1350
1400
1450

Fig(8)

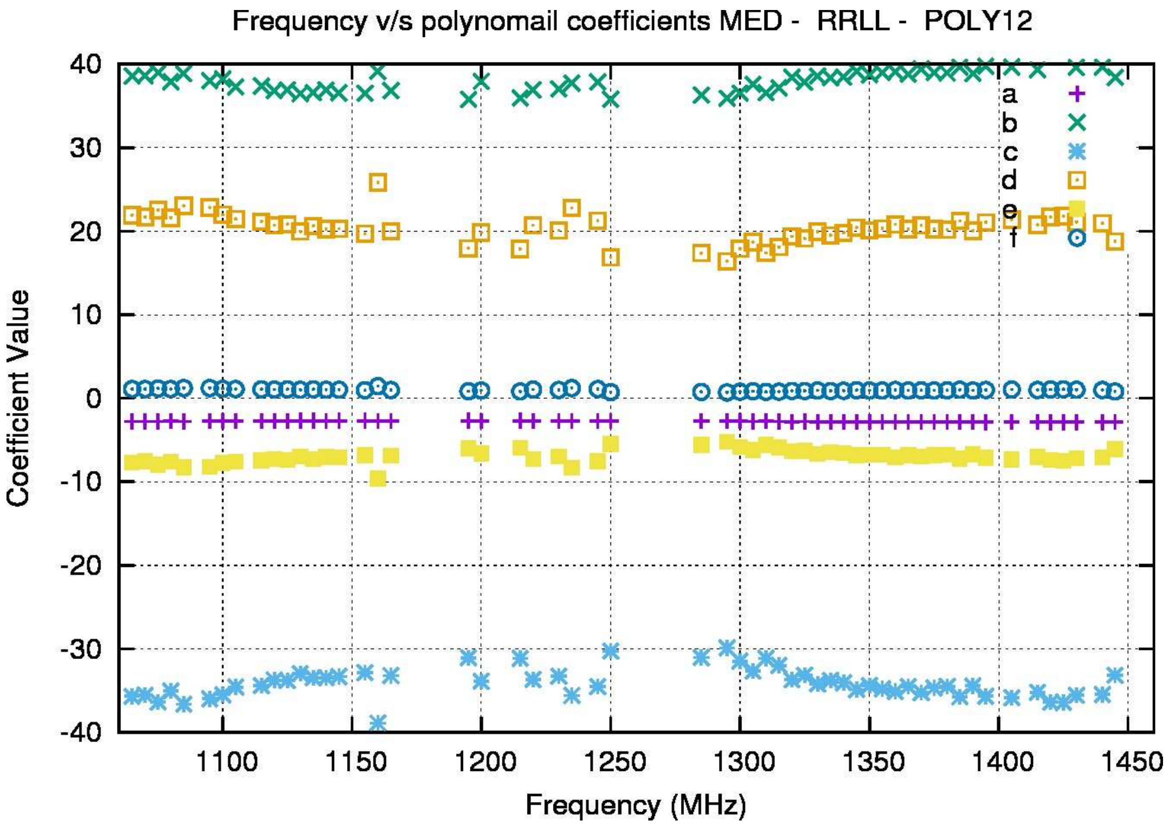

Fig(9)

Accuracy of the parametrization of the primary beam

In order to get an idea as to the expected accuracy of the primary beam correction, tje RMS value of the difference between the median beam as well as the MAXimum value of the (absolute) difference was computed over both rings and annuli centered at the beam maximum. Fig(10) show the rings and surface shapes used for this analysis. The sizes for the rings are annuli scale with the HPBW (for e.g. if HPBW = 24', then 50% =12', 100% = 24', and 200% = 48'). The RMS and MAX values are computed for both the difference between the data and the polynomial models as well as the difference normalized by the model value at that location. The values for the 12th order polynomial are also plotted and tabulated for different rings and annuli. These plots and table should give the user an indication of the expected error on the primary beam correction to the flux.

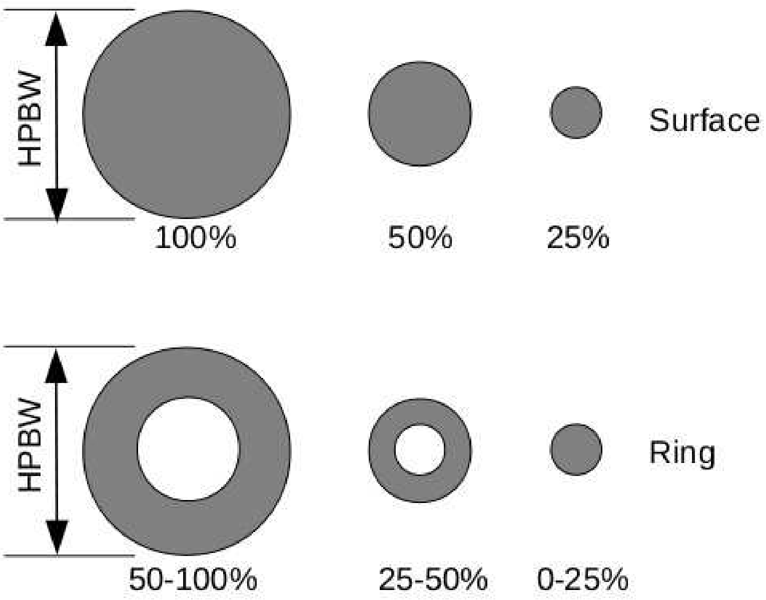

Fig(10)

Fig (11) and Fig(12) shows the comparison between 8th order, 10th order and 12th order polynomial fits.

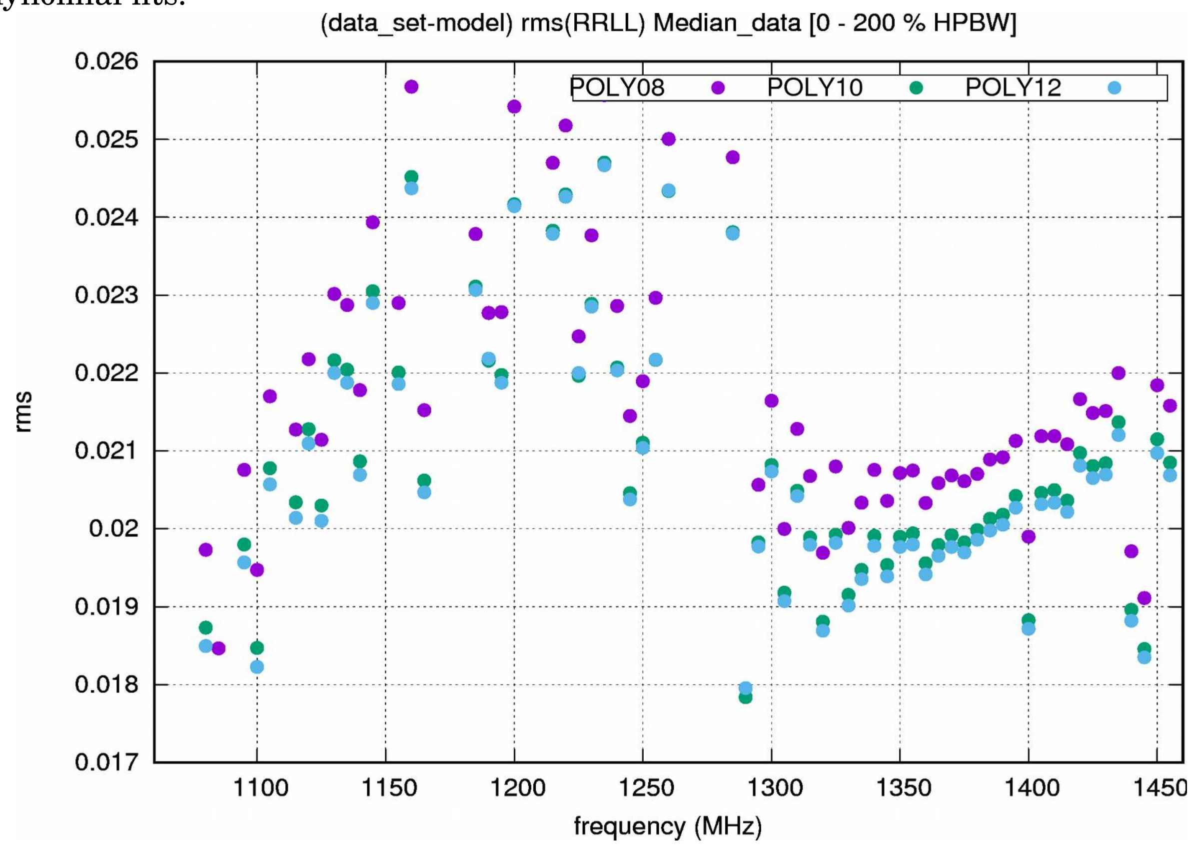

Fig(11)

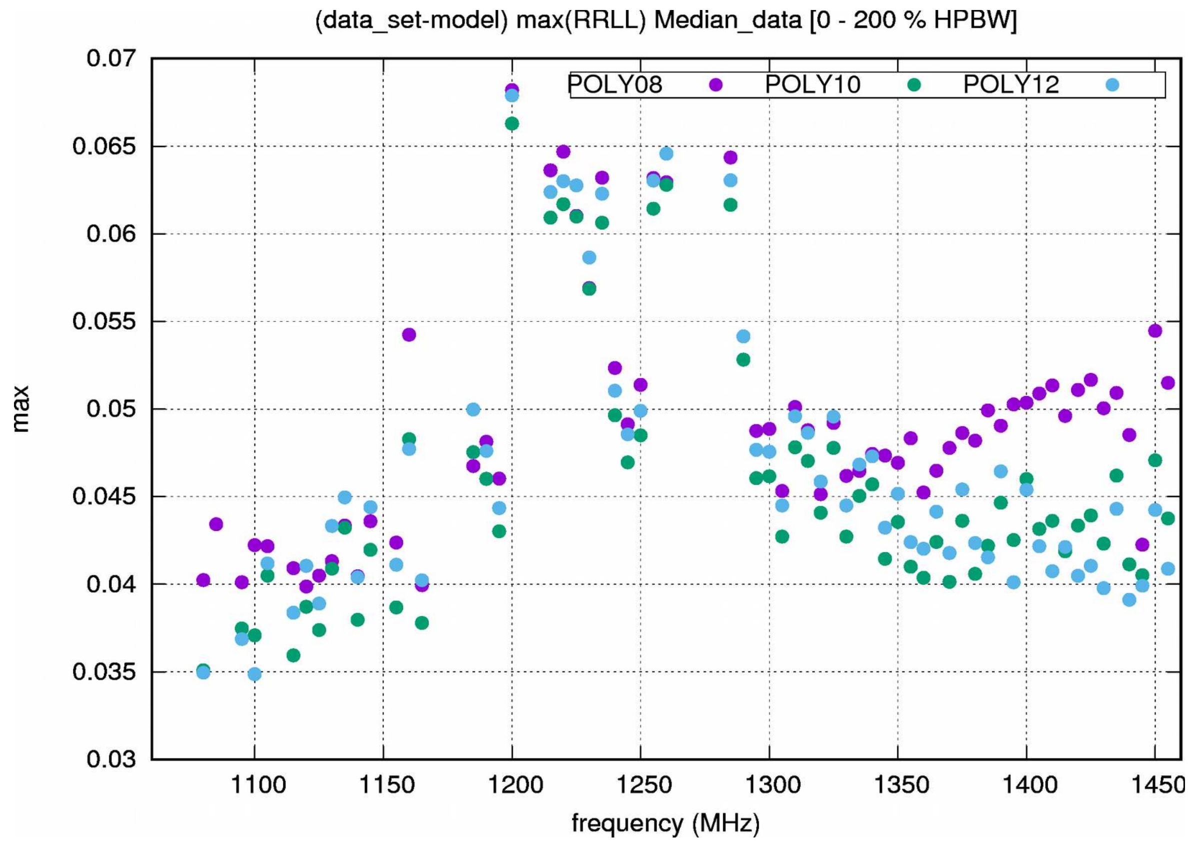
(data_set-model) max(RRLL) Median_data [0 - 200 % HPBW]
POLY08
POLY10
POLY12
max
0.07
0.065
0.06
0.055
0.05
0.045
0.04
0.035
0.03
1100
1150
1200
1250
1300
1350
1400
1450
frequency (MHz)

Fig(12)

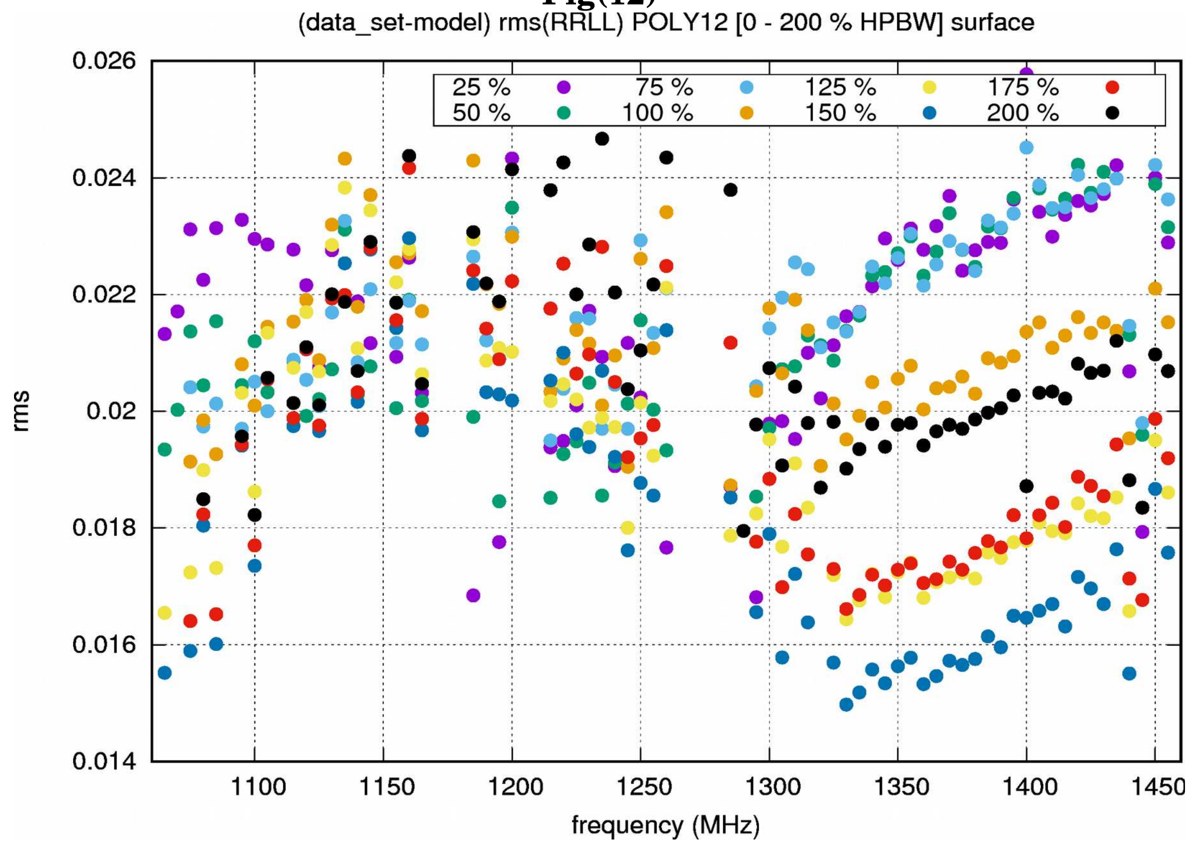
(data_set-model) rms(RRLL) POLY12 [0 - 200 % HPBW] surface
25 %
50 %
75 %
100 %
125 %
150 %
175 %
200 %
rms
0.026
0.024
0.022
0.02
0.018
0.016
0.014
1100
1150
1200
1250
1300
1350
1400
1450
frequency (MHz)

Fig(13)

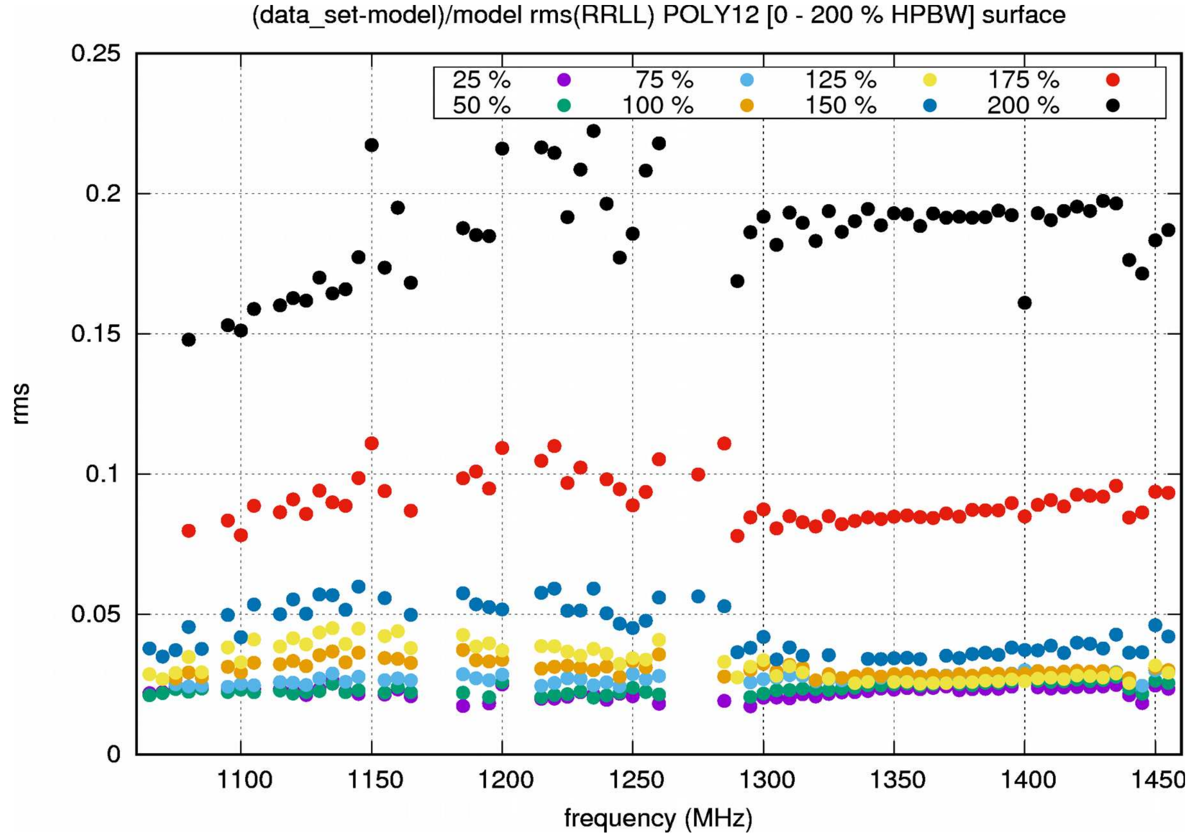
(data_set-model)/model rms(RRLL) POLY12 [0 - 200 % HPBW] surface
25 %
50 %
75 %
100 %
125 %
150 %
175 %
200 %
rms
frequency (MHz)

Fig(14)

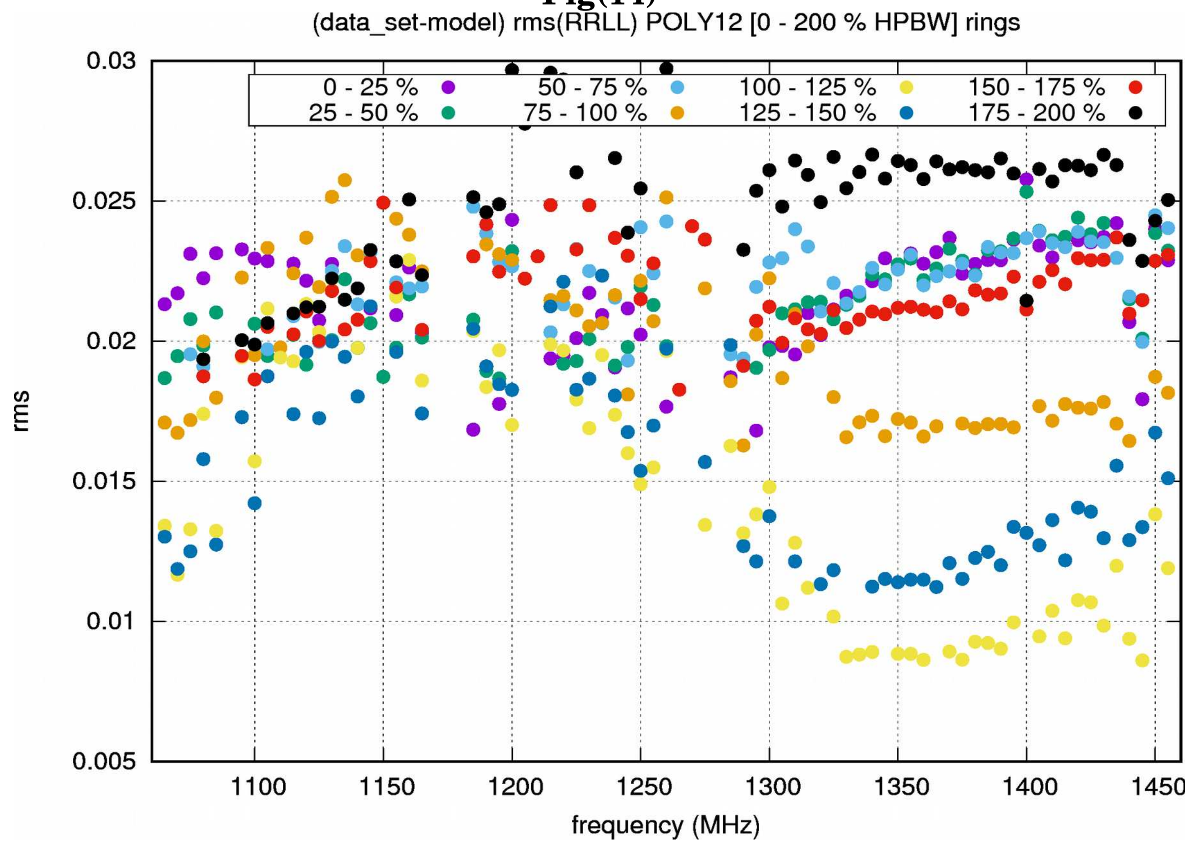
(data_set-model) rms(RRLL) POLY12 [0 - 200 % HPBW] rings
0 - 25 %
25 - 50 %
50 - 75 %
75 - 100 %
100 - 125 %
125 - 150 %
150 - 175 %
175 - 200 %
rms
frequency (MHz)

Fig(15)

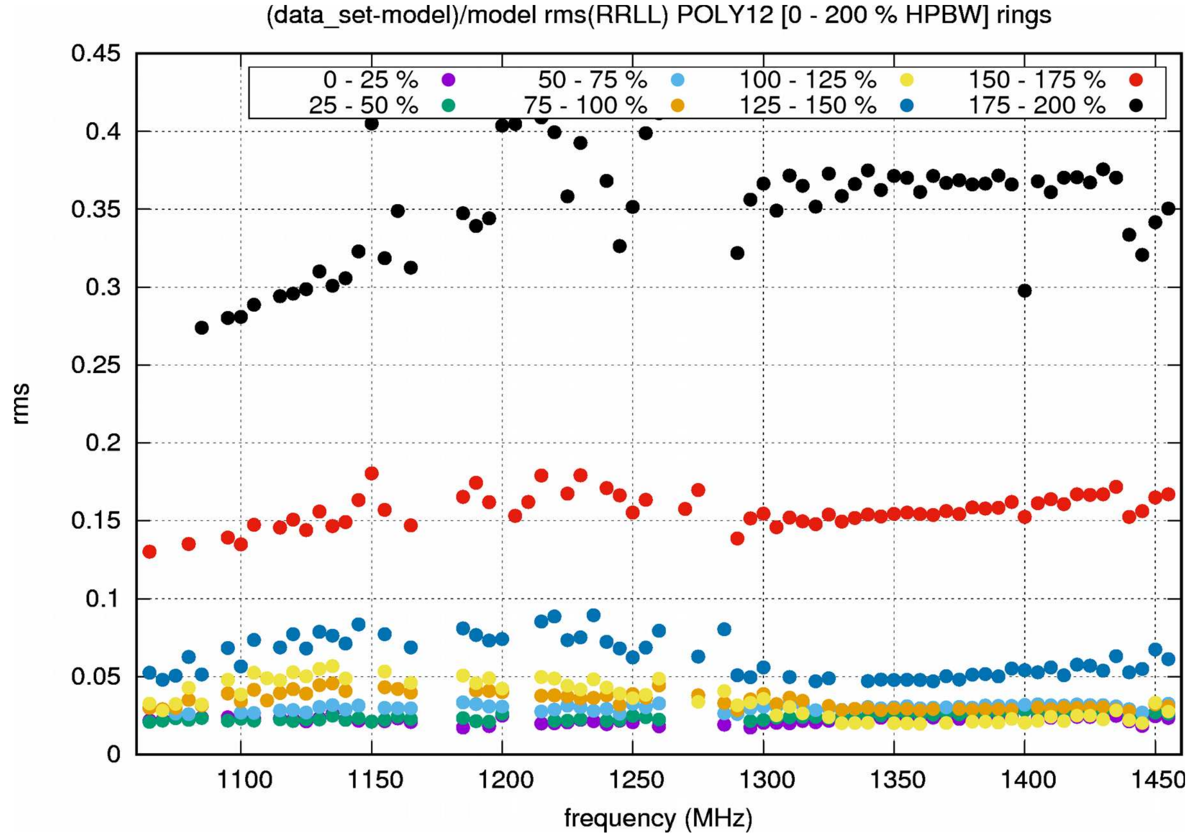

Fig(16)

Fig(13) and Fig(14) shows the comparison between the various surfaces unnormalized RMS values of 12^{th} order polynomial fit.

Fig(15) and Fig(16) shows the comparison between the various rings normalized RMS values of 12^{th} order polynomial fit.

Conclusions:

Polynomial Coefficients @ L band

Order	Polynomial Coefficients					
	a	**b**	**c**	**d**	**e**	**f**
8^{th}	-2.6143567	27.5937122	-13.267957	2.39478824		
10^{th}	-2.7480967	34.2057392	-23.736563	8.98288122	-1.4282202	
12^{th}	-2.8122849	38.7074017	-34.371800	20.1072777	-6.7313771	0.93962093

RMS values for (data_set – model) [200%] HPBW

Polynomial	RMS
8^{th} order	0.0213
10^{th} order	0.0205
12^{th} order	0.0204

RMS values for (data-set – model) [0-200%] HPBW, surfaces

Surfaces for 12^{th} Order	RMS
25 %	0.0222
50 %	0.0212
75 %	0.0219
100 %	0.0211
125 %	0.0185
150 %	0.0176
175 %	0.0188
200 %	0.0204

RMS values for (data-set – model) [0-200%] HPBW, rings

Rings for 12^{th} Order	RMS
0 - 25 %	0.0222
25 - 50 %	0.0211
50 - 75 %	0.0225
75 - 100 %	0.0287
100 - 125 %	0.0134
125 - 150 %	0.0142
150 - 175 %	0.0215
175 - 200 %	0.0258